Journal of Applied Fluid Mechanics, Vol. 8, No. 2, pp. 281-290, 2015.
Available online at www.jafmonline.net, ISSN 1735-3572, EISSN 1735-3645.
DOI: 10.18869/acadpub.jafm.67.221.21446

Interaction between the Flow in Two Nearby Pores within a Porous Material during Transitional and Turbulent Flow

S. Khayamyan† and T. S. Lundström

Division of Fluid Mechanics, Luleå University of Technology, Luleå, SE-971 87, Sweden

†*Corresponding Author Email: shekha@ltu.se*

(Received Aug 29, 2013; accepted April 7, 2014)

ABSTRACT

The transition from laminar to turbulent flow in porous media is studied with a pore doublet model consisting of pipes with different diameter. The pressure drop over all pipes is recorded by pressure transducers for different flow rates. Results show that the flow in the parallel pipes is redistributed when turbulent slugs pass through one of them and six different flow zones were identified by studying the difference between the Re in the parallel pipes. Each flow zone starts when the flow regime of one of the pipe changes. Transitional flow of each pipe increases the correlation between different pipes pressure drop fluctuations. Frequency analysis of the pressure drops show that the larger pipe makes the system to oscillate by the presence of turbulent patches in its flow. However, when the flow in the smaller pipe enters into the transitional zone the larger pipe starts to follow the fluctuations of the smaller pipe.

Keywords: Porous media, Transitional flow, Turbulent flow, Pore doublet model, Pipe flow.

NOMENCLATURE

b	adjusting coefficient	P_{xx}	frequency content
d	differentiation sign	PMMA	poly methyl methacrylate
D	diameter	Q	mass flow rate
e	pipe roughness	Re	Reynolds number
f	friction factor, frequency	Re_{diff}	difference between Re
H	header pipe	S	smaller pipe
i	dummy variable	t	time
k	adjusting coefficient	u	velocity
K	permeability	w	weight
L	length, larger pipe	x_i	i^{th} data point
m	adjusting coefficient	$X(f)$	fourier transform of x(t)
m_n	normalized nth momentum	$\overline{x}$	mean value of data series
M_n	data nth momentum	$\overline{X(f)}$	conjugate of $X(f)$
M_2	data variance	y(t)	data point at moment (t)
m°	mass flow rate	Δ	difference operator
N	number of data point	μ	dynamic viscosity
P	pressure	ρ	density

1 INTRODUCTION

Transitional flow is one of the most challenging problems of fluid mechanics, especially in porous media due to the often complex geometry encountered by the fluid. The first relationship describing fluid flow within porous media was based on Darcy's pioneering experimental work on packed beds Darcy (1856). The by these experiments derived Darcy law ($u = \Delta p/L \cdot K/\mu$) states that the superficial velocity (u) is proportional to the pressure drop along a porous bed ($\Delta p/L$) where L, μ and K are the length of the porous bed, the dynamic viscosity and the permeability respectively. Darcy's empirical law can be derived from the governing equations, i.e. the Navier–Stokes and continuity equations, by homogenization techniques Sanchez-Palencia (1980) or volume averaging

techniques Whitaker (1986). Darcy's law is often said to be valid for Stokes flow Re < 1 (Lindquist 1933, Schneebeli 1955, Hubbert 1956, Scheidegger 1960, Chauveteau and Thirriot 1967), but Hellstrom et al. (2010) have shown that it can be valid up to particle Reynolds number, Re ≈ 10. The actual limiting value is dependent on how Re is defined. In 1863 Dupuit noticed that the linear Darcy's law does not represent experimental data at higher flow rates. Following this observation Forchheimer (1901), added a quadratic correction term to Darcy's law in order to capture the behavior of the experimental data at higher Re. Later on other correction terms were proposed (Chauveteau 1967, Muskat 1946, Skjetne 1999) and finally Darcy's law was modified to the so called Ergun-Forchheimer equation that may be written in the following form: $\Delta p/L = \mu/k\cdot(u + bu^m)$ where k, b and m are variables that should be chosen in a way that the equation fits to experimental data. By doing this the Equation captures the behavior of experimental data for Re > 10 (Seguin 1998, Comiti 2000, Papathanasiou 2001).

Several mechanisms have been suggested to cause the deviation from Darcy's law such as:

- Loss of kinetic energy due to contraction and expansion of pore space Panfilov (2006)
- The effect of pore solid boundaries on pressure loss Hayes (1996)
- Microscopic inertial forces presented in the drag forces Ma (1993)
- Formation of inertia flows at the center of pores Dybbs (1984)
- Formation of a viscous boundary layer Whitaker (1996)
- The interstitial drag force (Hassanizadeh and Gray 1987, Ma and Ruth 1993)
- Singularity of streamline patterns Panfilov et al. (2003)
- Separation of flow (Skjetne and Auriault 1999b)
- Deformation of streamline patterns and formation of eddies (Fourar et al. 2004, McClure et al. 2010, Panfilov and Fourar 2006)

This, in essence, tells us that inertial forces result in the breakdown of Darcy's law at modest Re. However, at higher flow rates the flow eventually will become fully turbulent. The transition from inertia dominated to turbulent flow, which is proven to be continuous based on experimental data, can macroscopically be approximated by Forchheimer equation or extended forms of it Nemec (2005). Notice that this implies a continuous transition from laminar to turbulent flow Hellström (2010) that differentiates porous media flow from pipe flow where there is a non-continuous transition from laminar to turbulent flow Joseph and Yang (2010). Different authors have reported the presence of turbulence on pore scale Hlushkou (2006) but the effect of pore geometry on the actual state or distribution of turbulence has not been studied in detailed. For regular packing turbulence appears in all the neighboring pores at the same time. In fully random packing where there is no control of position or size of the pores formed the detailed geometry of most of neighboring pores affect the flow. Simplified geometries such as a unit cell (Wan 1996; Nordlund 2009) and a pore-doublet (Rose 1956; Sorbie 1995; Lundström 2008; Khayamyan et al. 2014) have been used to distill the geometrical effect. Following this trend we will continue to study the pore-doublet model presented in Khayamyan et al. 2013. This model was applied in order to take advantage of the well-studied pipe flow e.g. (Reynolds (1883), Wygnanski 1973, Gustavsson 1991).

In a previous study, Khayamyan et al. (2013), it was shown that the flow in the pipes is redistributed when transient slugs pass through one of them. The presence of the slugs in the pipes is revealed by positive skewness as well as an increase of the standard deviation of the pressure drops and correlation between pipes pressure drops. In the present paper the experimental investigation is considerably increased to higher Reynolds numbers and each measurement is done in a more proper way. The frequency content of the data is scrutinized and the results are interpreted in terms of a general porous media.

2. EXPERIMENTAL SETUP AND PROCEDURE

The flow around one particle within a porous medium is studied with a pore-doublet setup, see Khayamyan et al. (2014) for details. The flow geometry is represented by two straight and parallel glass pipes with diameters of 4.05 and 3.02 mm and lengths of 1100 mm. Water is supplied to the pipes from a third glass pipe with diameter of 9.05 mm and length of 750 mm connected via a Y-shaped splitter as shown in Fig. 1 & 2. The splitter is made of PMMA by machining the branches to 8 mm diameter. The angle between the branches is 50º, cf. Fig. 3. In order to keep the pipes horizontal and parallel they are aligned to an aluminum bar. The flow from the parallel pipes runs into two boxes. These two boxes and also the sliding tank providing the water to the pipes are of over-flow type so that the parallel pipes have equal pressure at their outlet and the driving pressure is kept constant during each run of the experiment.

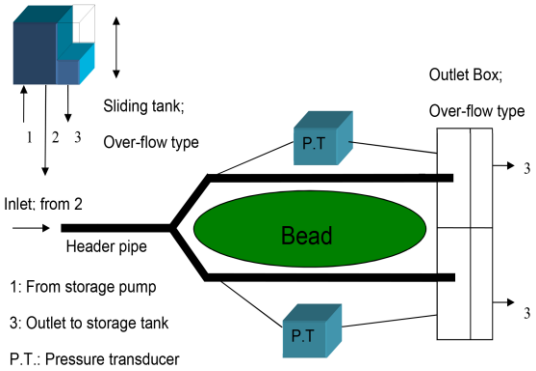

Fig. 1. Schematic drawing of flow model and experimental setup

Each of the parallel pipes has pressure tap holes d = 1 mm positioned 20 mm after the splitter. There are also two pressure tap holes on the header pipe placed 700 mm from each other. Three differential pressure

transducers are used to record the pressure drop over each pipe during each run of the experiment. The transducers for the parallel and header pipes are from the OMEGA PX2300 series and LPM/LPX1000 series, respectively.

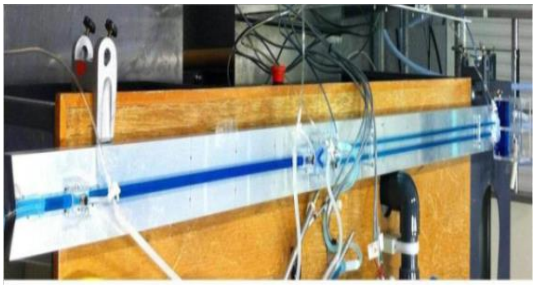

Fig. 2. Experimental setup showing from the left, the header pipe in blue, the Y-splitter, the parallel pipes also in blue and the outlet box.

Each experiment was run during 60 minutes and the analog pressure drop signals from the pipes were converted to digital signals by an A/D converter and recoded with Signal Express into a computer at 40 Hz.

The flow rate through each parallel pipe was measured by collecting water 10 times for 60 seconds. The flow rate through the header pipe was then derived by usage of (1). The water temperature was 20° ± 0.1° during all runs. The position of the sliding tank was varied in a series of 144 runs with the header pipe Re, Re_H, varying from 1100 to 3700.

2 Theory

For the system of pipes studied continuity yields that

$Q_L + Q_S = Q_H$,

and thus (1)

$(D\,Re)_L + (D\,Re)_S = (D\,Re)_H$,

subscripts L, S and H refer to larger, smaller and header pipes respectively. The characteristic length scales for each pipe is its diameter. It is now assumed that the pressure drop from the splitter over the parallel pipes down to the free surface in the outlet box is identical. Thus for the two pipes,

$$\Delta P_L = \Delta P_S. \quad (2)$$

The pressure drop, ΔP in each section consists of a number of minor losses (which will be discussed later on) and a straight pipe loss which may be expressed as

$$\Delta P = f\frac{L}{D}\frac{\rho U^2}{2} = f\,\frac{L}{D}\frac{\mu^2}{2D^2\rho}Re^2, \quad (3)$$

Where L is the length of the pipe, U the mean velocity and f the friction factor, which is a function of Re Çengel and Cimbala (2010).

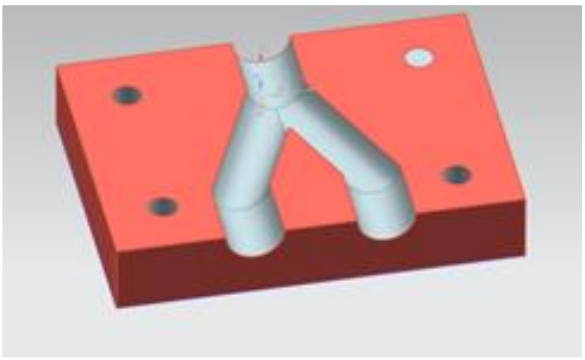

Fig. 3. The Y-splitter section

3 Methods of Evaluation

3.1 Statistical Analysis

The collected pressure data were processed in several ways and will be presented as

- Time averages and higher statistical moments (rms and skewness)
- Time series
- Correlations

The data presentation is a mixture between time averages and time resolved data. The ambition is to explain some of the statistical behavior from the time series which should better reflect the actual physical processes. The time average is defined as

$$\overline{x} = \frac{\sum_{i=1}^{N} x_i}{N}, \quad (4)$$

Where N is the number of samples. The higher statistical moments are defined as

$$M_n = \frac{\sum_{i=1}^{N}(x_i - \overline{x})^n}{N}, \quad \text{where } n = 2, 3, \ldots \quad (5)$$

In this equation, $n = 2$ gives the variance and $n = 3$ the skewness. The standard deviation is the square root of the variance and is denoted rms. The skewness is normalized with the variance via

$$m_n = \frac{M_n}{\sqrt{(M_2)^n}}, \quad \text{Where } n = 3. \quad (6)$$

For the correlation, the Pearson correlation coefficient is applied to detect the relation between the pressure drops in the two pipes according to

$$Correlation = \frac{\Sigma(x-\overline{x})(y-\overline{y})}{\sqrt{(M_{2,\,x})(M_{2,\,y})}}. \quad (7)$$

3.2 Frequency Domain Analysis

The experiments will yield time series of pressure. The relationship between two sets of time series, *x(t)* and *y(t)*, can be scrutinized by computing the power spectral density function of the time series data, the gain factor, the phase difference and the coherency function. All of these methods are based on Fast Fourier Transform (FFT) of the time series data according to:

$$X(f) = \int_0^\infty x(t) e^{-i\,2\pi f t}\, dt\,, \tag{8}$$

Where X is data in the frequency plane, x the data in the real plane, f is frequency and t time.

3.3 Power Spectral Density Function

The power spectral density (PSD) is simply defined as:

$$P_{xx} = |X(f)|^2 = X(f) * \overline{X(f)}\,. \tag{9}$$

The usage of this function is a practical way to recognize oscillatory signals in time series data. The function may also be used to find the amplitudes and the frequencies of the oscillations. PSD originally breaks down time series data into sets of sinusoidal waves of different frequencies and presents the strength or the energy of the signal at each frequency. The unit of PSD is energy per frequency and the energy of a frequency band is the area under the PSD plot within that frequency range.

3.4 Gain Factor

The gain factor, or the magnitude of the frequency response function, is the ratio of the Fourier transform of the data from two time series according to:

$$Gain\ factor = \left|\frac{X(f)}{Y(f)}\right|. \tag{10}$$

Hence it tells us which time series that dominates at a certain frequency.

The gain factor may disclose a correspondence between two sets of time series data and if they are following common trends. The important point to consider is that, even if the gain factor detect that there are common trends in the data, the trends may be of second order since the amplitudes of the variations might be small. Therefore, it is essential to investigate, at least, the power spectral density of one of the time series data to make sure that the amplitude of the coherent variations is large enough.

4 RESULTS

4.1 Statistical Analysis

The flow through the parallel pipes is first evaluated as a function of Re_H; cf. Fig. 4. The open symbols are from the current study and the filled from Khayamyan et al. (2014). Overall, the two series are in good agreement and the results from the two experimental series overlap in the laminar regime and also at the inflection point at $Re_H \approx 2000$. There are, however, some differences just after the inflation point. The maximum difference between the series for the larger and the smaller pipes are 2.1% and 8.1% which occur at $Re_H \approx 1800$ & 1750 respectively. These discrepancies may reflect the improved accuracy in the measurements (flow rate measured for longer time, from 10 (s) to 60 (s), more repetitions 4 times to 10 times and better temperature control). This indicates that the data in the second series are more reliable and they also cover larger range of Re_H. Hence focus is now set on the second series of experiments.

When comparing $Re_{L,S}$ as a function of Re_H for the parallel pipes it is obvious that there is a redistribution of the percentage flow between the pipes. Since the pipes face the same pressure drop the change in the slope of the curves is the result of alterations of the overall friction within the pipes when the flow changes characteristics.

To investigate this further, the difference between Re of the two parallel pipes, Re_{diff}, is derived and plotted in Fig. 4. Based on the variation of the slope of this curve six ranges can be identified for which the flow regimes in the pipe network can be analyzed. In the first range (Range 1), $Re_H \lesssim 1500$, the flow is laminar in both pipes. Re_{diff} may therefore be expressed as:

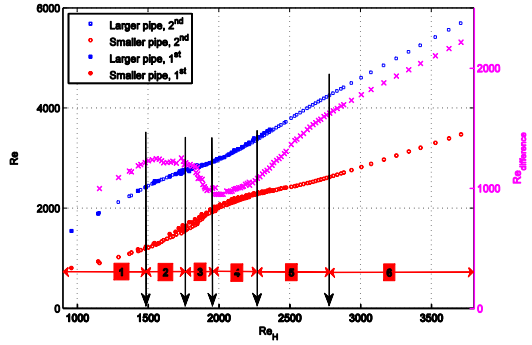

Fig. 4. Reynolds number for the two parallel pipes as a function of Re_H.

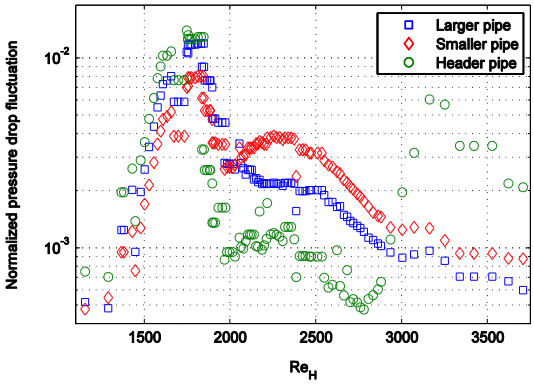

Fig. 5. Normalized standard deviation of pressure drop along parallel pipes

$$Re_{diff} = Re_L - Re_s = \frac{1 - \left(\frac{D_S}{D_L}\right)^3}{1 + \left(\frac{D_S}{D_L}\right)^4} \frac{D_H}{D_L} Re_H\,, \tag{11}$$

using (3) and assuming that the laminar flow is fully developed in all pipes, hence

$$f = \frac{64}{Re}, \tag{12}$$

which is generally true for Re < 2000. Using this relationship the slope of the curve Re_{diff} may readily be calculated to 1.0 (i.e. when only considering friction at the walls of the pipes) while the experimental data in Fig. 4 yields a slope of 0.68. However, when adding losses due to the bends in the splitter, the inlet and

outlet losses of the pipes and losses due to entrance length effects the slope is calculated to 0.73 which is much closer to the experimental value. This reveals that it is necessary to take into account all losses to have better estimation of flow distribution. By scrutinizing the slope of Re_{diff} additional ranges can be defined. Range 2, 1500 <Re_H< 1800, where Re_{diff} is constant, Range 3, 1800 <Re_H≲ 2000 where Re_{diff} decreases, Range 4, 2000 ≲Re_H< 2300, with a slight increase in Re_{diff}, Range 5, 2300 <Re_H< 2800, where Re_{diff} increases rapidly and Range 6, Re_H> 2800, where the slope of Re_{diff} becomes somewhat smaller than in Range 5. The reasons for the changes in the slope of Re_{diff} were partly explained in Khayamyan et al. (2014) and will be further analyzed in this investigation.

Table 1 Flow regimes based on ReH

Pipe	$Re_{H,\ Laminar}$	$Re_{H,\ Transient}$	$Re_{H,\ Turbulent}$
Header	2750	2750 – 3200	3200
Larger	1500	1500 – 1800	1800
Smaller	2000	2000 - 2300	2300

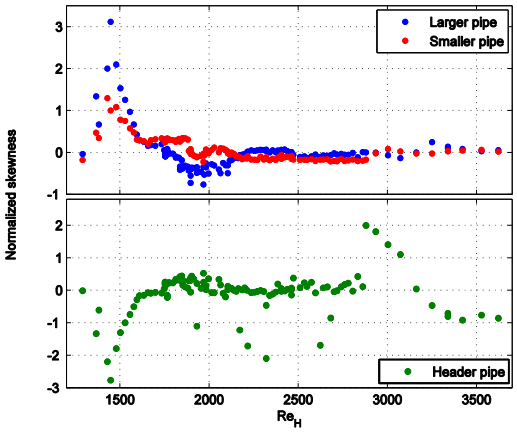

Fig. 6a. Normalized skewness of pressure drop from two experiments

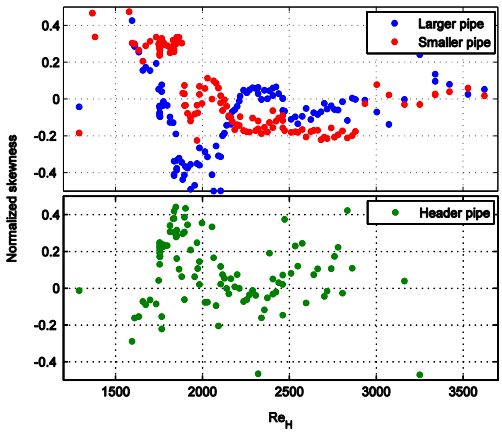

Fig. 6b. The enlarged view of normalized skewness around its zero

Let us now study the statistics of the pressure measurements and start with the pressure fluctuations in the form of the root mean square of the pressure drop normalized with mean pressure, $NRMS_P$, see Fig. 5. As is obvious from Fig. 4, for a certain flow rate Re_L is larger than both Re_S and Re_H and the flow in the larger pipe may become turbulent already at Re_H = 1200. This is also reflected in the pressure fluctuations which increase rapidly from about this value of Re_H. For Re_H< 2000 (Ranges 1-3) the $NRMS_P$, of the header and the smaller pipes are synchronized with that in the larger pipe. This is probably due to that the momentum of the flow within the smaller and header pipes is not enough to resist the pressure fluctuations generated in the larger pipe.

For 2000 <Re_H< 2800 (Ranges 4 & 5) the most important behavior of the $NRMS_P$ is that at $Re_H \approx 2000$ the $NRMS_P$ of the smaller pipe ceases to follow the trends of the $NRMS_P$ of the larger pipe. It instead exceeds the $NRMS_P$ of the larger pipe and continues to be larger for the rest of its range with a maximum at $Re_H \approx 2350$. At $Re_H \approx 2800$ (the start of Range 6) the $NRMS_P$ of the header pipe starts to increase. This is an indication of transitional flow in the header pipe which is not directly reflected in the $NRMS_P$ of the parallel pipes that continue to decrease until $Re_H \approx 3000$. The parallel pipes are in the fully turbulent regime and they do not follow the pressure disturbances in the header pipe.

When turbulent structures show up in a pipe there will be positive pressure peaks in the pressure drop along the pipe. Such features are disclosed by plotting the skewness for which the effect of smaller and symmetrically distributed amplitude fluctuations diminishes and larger, one-sided fluctuations are amplified. Figure 6a presents the normalized skewness of the pressure measurements in this study. Since most of the skewness values are concentrated around the x-axis, Fig. 6b focuses more on this part. As seen the skewness deviates from zero due to pressure fluctuations of the larger pipe at $Re_H \approx 1300$ and it reaches its peak at $Re_H \approx 1500$. Hence the start of the transition is not reflected in any major redistribution of the flow since Range 2 when Re_{diff} becomes constant start at $Re_H \approx 1500$. The skewness of the header pipe behaves in an opposite manner, cf. Fig. 6a, and has negative values in this range to compensate the positive peaks in the parallel pipes (the total pressure drop is constant). After $Re_H \approx 1500$ the skewness of all three pipes go towards zero and at the end of Range 2 ($Re_H \approx$ 1800) both the larger pipe and the header pipe have almost zero skewness, cf. Fig. 6b. Before entering into Range 4, $Re_H \approx 1900$, the skewness of the smaller pipe deviates from the larger pipe. It starts to grow and has its maximum at $Re_H \approx 2050$. The smaller pipes' positive skewness shows that its pressure drop distribution has positive peaks that can be traced to the presence of turbulent slugs in its flow.

As before, the header pipe follows these pressure fluctuations since it does not have enough momentum to resist it. At $Re_H \approx 2800$ (start of Range 6) the header pipes skewness starts to grow and reaches its maximum around $Re_H \approx 2880$. The positive skewness within the header pipe does not have any noticeable effect on the flow in the parallel pipes.

To summarize, at $Re_H \approx 1500$ (start of Range 2) the flow in the larger pipe becomes transitional which is

denoted by increase in skewness and in the $NRMS_P$, see Table 1. The pressure fluctuations in the larger pipe are reflected in the other two pipes where the flow is laminar. The flow in the larger pipe enters into the fully turbulent regime at $Re_H \approx 1800$ (start of Range 3) since its skewness goes to zero and $NRMS_P$ starts to decrease. Later, at $Re_H \approx 2000$ (start of Range 4) the flow in the smaller pipe becomes transitional since its $NRMS_P$ and skewness grows. The flow in the smaller pipe enters into the fully turbulent regime at $Re_H \approx 2300$ (start of Range 5) and the level of its $NRMS_P$ decreases. Finally at $Re_H \approx 2800$ (start of Range 6), the flow in the header pipe becomes transitional and its skewness and $NRMS_P$ grows. At $Re_H \approx 3200$ the level of the pressure fluctuations reaches its maximum indicating a transfer

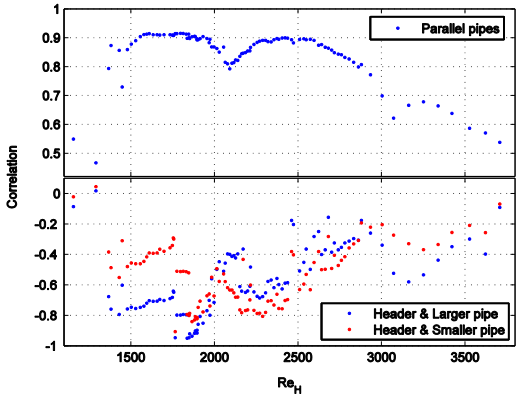

Fig. 7. The correlation of pressure drop between different pipes.

into fully turbulent flow in the header pipe. Another important issue is that $Re_H \geq Re_S$, cf. Fig. 4, but the flow in the smaller pipe and the header pipe become transitional at $Re_H \approx$ 2000 and 2800, respectively, cf. Fig. 4 & 5. This highlights the effect of the splitter and how it induces more disturbances at the inlet of both parallel pipes and triggers turbulent structures, puffs. This means Re is not the only parameter which determines the flow regime and the level of disturbances at the entrance of the pipe is an important factor as well.

With knowledge of the basic stages of the system studied it is also of interest to find out how the pressure fluctuations correlate. The correlation of the pressure drop between the parallel pipes is initially weak for Range 1, but as Re_H moves into Range 2 it has increases to a relatively high value, see Fig. 7. This implies that the correlation is, to start with, related to the turbulent spots disclosed by the skewness, cf. Fig. 6. In a similar manner the correlation values between any of the two parallel pipes and the header pipe increases. At Re_H between 1900 – 2100 (Range 2-3) the correlation between the parallel pipes decreases. Hence the initial pressure fluctuations in the smaller pipe, found by the skewness, are not transformed to the larger pipe. However, the fluctuations in the smaller pipe are immediately reflected in the header pipe, see the increase in correlation between these pipes at $Re_H \approx 2000$, Fig. 7. At $Re_H \approx 2900$ the correlations between the header pipe and the parallel pipes reach a local minimum and then the correlation increases. Following the previous discussion this is due pressure fluctuations in the header pipe that actually start already at $Re_H \approx 2800$ but it does not impact the flow in the parallel pipes until $Re_H \approx 2900$, cf. Fig. 5. To summarize, pressure fluctuations caused by transitional flow are directly transferred to pipes with laminar flow. Such fluctuations are also eventually transferred to pipes with turbulent flow when the fluctuations become strong enough.

The slope of Re_{diff} for the two parallel pipes in the turbulent regime, $Re_H \gtrsim 2300$, is 0.21 by which only considers friction force from the walls of the pipes via Blasius' formula

$$f = \frac{0.316}{Re^{0.25}}. \tag{13}$$

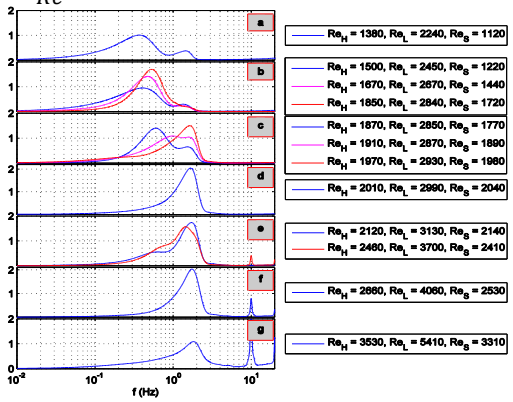

Fig. 8. Power spectra of pressure drop along the larger pipe for Re_H = 1380, 1500, 1670, 1850, 1870, 1910, 1970, 2010, 2120, 2460, 2660 and 3530

However, following the analysis of the laminar flow all sources to losses can be added to the calculations. When the pressure drop due to the other sources are included into the numerical calculation the slope of Re_{diff} will be 0.55 and 0.56 with Blasius and Colebrook friction factor, equations (13) and (14), respectively.

$$\frac{1}{\sqrt{f}} = -2.0 \log\left(\frac{e/D}{3.7} + \frac{2.51}{Re\sqrt{f}}\right). \tag{14}$$

The experimental data in Fig. 4 yields that Re_{diff} has two slopes in the turbulent regime which are 1.14 for Re_H between 2300 and 2800 (Range 5) and 0.62 for Re_H higher than 2800 (Range 6). The latter experimental slope is consequently rather close to the theoretically derived values. The larger slope of Re_{diff} for Range 5 means that a larger portion of the fluid passes the larger pipe in order to satisfy the equal pressure drop condition between the parallel pipes. This highlights the effect of the feeding flow into the parallel pipes because when laminar flow enters into pipes which are already in the turbulent regime it needs a distance for the turbulent structure to develop. The developing length should be longer for the larger pipe since the velocity is higher. Along the developing distance flow regimes are developing from laminar to transient and finally turbulent at the end of it which makes the friction factor of this length smaller compare to fully turbulent flow.

4.2 Frequency Analysis

Figures 8-9 present the non-dimensionalized power spectra of the pressure drop fluctuations normalized with the average energy of the fluctuations, $\frac{1}{2}p_{rms}^2$, for the larger and smaller pipe respectively.

Initially the power spectra have two peaks with relatively small amplitudes. This is an indication of turbulent patches in the flow which was already found by the skewness analysis, cf. Fig. 6a. At Re_H from 1500 to 1850 (appr. Range 2) the low frequency peak of both pipes spectrum become more powerful driven by an increased number of turbulent patches in the larger pipe, cf. Fig.s 8-9 part b.

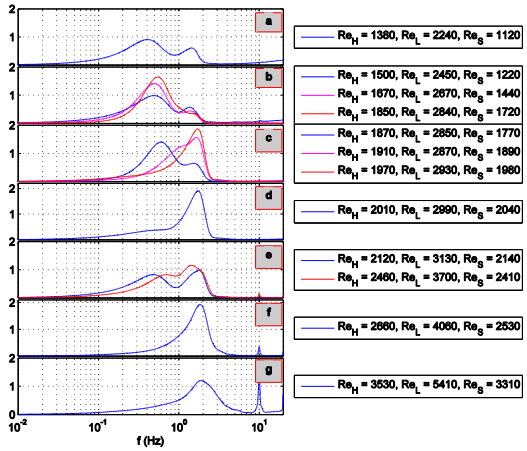

Fig. 9. Power spectra of pressure drop along the smaller pipe for Re_H = 1380, 1500, 1670, 1850, 1870, 1910, 1970, 2010, 2120, 2460, 2660 and 3530

When Re_H increases even more the low frequency peaks lose their power and move slightly to the right while the high frequency peaks gain power, cf. Fig. 8 part c (Range 3). The powerful high frequency fluctuations can distribute energy more uniformly among pressure drop oscillations therefore the level of fluctuations decreases within this range, cf. Fig. 5. In the range of Re_H 1980 - 2060 the spectrum of both pipes is dominated by the high frequency peak, cf. Fig.s 8d. The powerful high frequency fluctuations cause the level of fluctuations of both pipes to become almost equal in this range, cf. Fig. 5. Here, also the skewness of the smaller pipe grows from negative values to positive values, cf. Fig. 6b, which is a sign of initiation of turbulent patches in the flow.

For Re_H between 2120 and 2460 (appr. Range 4) turbulent spots form in the smaller pipe since a new low frequency peak appears in the spectrum of both pipes but more clearly in the smaller pipe, cf. Fig.s 8-9 e. For Re_H between 2570 and 2780 (within Range 5) the spectrum of both pipes again is dominated by high frequency peaks, cf. Fig.s 8-9 f. The powerful high frequency band fluctuations, as it was explained before, are connected to uniform distribution of energy which lowers the level of fluctuations in this range. For Re_H between 2800 and 3710 (Range 6) the spectrum of both pipes has only the high frequency peak and its power decreases by growth of the Re_H, cf. Fig.s 8-9 g.

Table 2 Error estimation of measured quantities for different pipe

	Re	Weight	Diameter	Pressure
Larger pipe	0.11%	0.03%	0.20%	0.25%
Smaller pipe	0.04%	0.07%	0.53%	0.25%
Header pipe	0.09%	0.02%	2.18%	0.25%

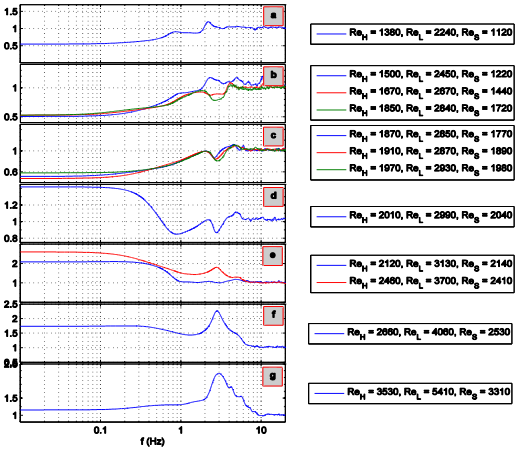

Fig. 10. Gain factor of pressure drop along parallel pipes for Re_H = 1380, 1500, 1670, 1850, 1870, 1910, 1970, 2010, 2120, 2460, 2660 and 3530.

Table 3 Error estimation of measured quantities

Quantity	Viscosity	Density	Time	Temperature
	2.56%	0.02%	1.0%	0.50%

Figure 10 presents the gain factor which is the square root of power ratio between two pipes; smaller/larger. For Re_H between 1150 and 1970 (Ranges 1-3) the gain factor is less than one, cf. Fig. 10a-c. This means that both frequency bands originate in the larger pipe and the smaller pipe just follows them. This is expected since in this range turbulent patches only pass through the larger pipe. The results also indicates that the high frequency fluctuations force both pipes to have almost equal amplitudes while low frequency fluctuations caused due to turbulent patches make fluctuations have different amplitudes.

For Re_H between 1980 and 2060 (Range 3-4) the gain factor at the low frequency band is more than unity which means that the low frequency band is caused by the smaller pipe fluctuations while the larger pipe causes the high frequency fluctuations, see Fig. 10d. Notice that the fluctuations in the smaller pipe could not be revealed from Fig. 8-9d. At Re_H between 2120 and 3710 (Range 4-6) the gain factor is more than unity in the whole frequency range which means that all fluctuations are governed from the smaller pipe. This explains why the level of fluctuations of the smaller pipe is higher than the level in the larger pipe at Re_H> 2120, cf. Fig. 5. At Re_H between and 2810 and 3710 there is no sign of low band frequency events which are associated with the presence of turbulent patches and the gain factor has almost constant value at the low band. However, it starts to grow at high frequency band

and it reaches its maximum at $f \approx 3$ (Hz) where however the power spectra is weak.

5.3 Estimation of Experimental Error

The average errors of measured quantities which are different for each pipe are listed in table 2. Also the error estimation of the general quantities of the experiment is listed in the table 3.

In order to see the effect of above mentioned quantities the following analysis is performed by using Taylor expansion.

Table 4 Error estimation of the measured variable on flow rate and Re

	Smaller pipe	Larger pipe	Header pipe
Error estimate of flow rate (m°)	0.94%	0.96%	0.97%
Error estimate of Re	1.69%	1.39%	1.94%

$$Re = \frac{\rho\, U\, D}{\mu}, \tag{15}$$

$$m^\circ = \rho\, U\, A, \tag{16}$$

$$Re = \frac{4}{\pi}\frac{m^\circ}{D\,\mu}, \tag{17}$$

$$dRe = \frac{4}{\pi}\frac{dm^\circ\, D\,\mu - m^\circ\,(dD\,\mu + D\,d\mu)}{(D\,\mu)^2}, \tag{18}$$

$$m^\circ = \frac{w}{t}, \tag{19}$$

$$dm^\circ = \frac{t\,dw - w\,dt}{t^2}. \tag{20}$$

The results of the analysis are listed in following table.

6. Application to Porous Media Flow

In flow through porous media the Ergun equation can be fitted to experiments with very good agreement. From this Equation a so called Blake type of friction factor can be defined as:

$$f' = 1.75 + \frac{150}{Re'}, \tag{21}$$

where Re is based on the hydraulic diameter of the porous media. As obvious from (21) f' approaches a constant value as Re' increases, see Fig. 11. If we now treat the parallel pipes as a system its friction factor may be plotted and compared to the ones for the single pipes and f' by usage of an equivalent diameter. As seen in Fig. 12 the system curve takes a form closer to the Ergun equation (f') as compared to f for the single pipes. This indicates that the continuous behavior seen in the experimental data can be traced to the mechanisms clarified in this work. It must, however, be noticed that the leveling out of the friction factor which indicated the start of turbulence takes place at a much higher Re for f than for f'. This is a topic for further studies and may be traced to the often very complex flow geometry in a porous media. The critical transitional Re is very much dependent on the flow conditions and is, for instance, around 370 for couette flow, see Dou and Khoo (2011).

7. Conclusion

Six flow zones are identified. Each zone marks the change of flow regime in one of the three pipes. Knowing the flow regime in each pipe is important information for analyzing the pressure drop signals and interpreting them. The effect of the feeding flow regime into the parallel pipes is identified since transition in the header pipe results in a new flow distribution in the system. The numerical solution of the system highlights the importance of minor pressure losses in the splitter which could be the same in real porous media.

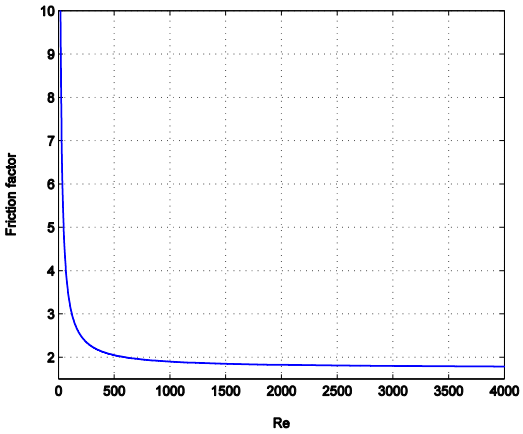

Fig. 11. Blake type of friction factor

Correlation between parallel pipes fluctuations grows when any of them becomes transitional, but correlation decreases when the pipe becomes turbulent. The header pipe is more correlated with larger pipe when it causes fluctuations, $Re_H < 2000$. However at $Re_H > 2000$ where the smaller pipe causes the fluctuations the header pipe follows the smaller pipe. At $Re_H > 2800$ where the header pipe becomes transitional it follows the larger pipe better.

The frequency analysis revealed two distinct events in the pressure drop signals of the parallel pipes, low and high band frequency fluctuations. Low band frequency fluctuations are caused by presence of turbulent patches in the flow. The presence of low frequency patches are even present in low Re flow, $Re_H < 1500$, but they are not as powerful as at higher Re.

The presence of turbulent patches causes fluctuations with low band frequencies. The gain factor shows that until $Re_H \approx 2000$ frequency fluctuations on both bands are triggered from the larger pipe. However, at $Re_H > 2000$ where the smaller pipe starts to become transitional the flow in the smaller pipe causes all fluctuations.

The gain factor depending on Re_H has values different than unity in low band frequency which makes parallel

pipes fluctuate with different amplitudes than each other. However, in the high frequency band the gain factor goes towards unity and tries to equalize the amplitudes of both pipes fluctuations. During transition there are two kind of fluctuations in the system; low band frequency fluctuations which disturbing the system and high band frequency fluctuations which tries to return the system back to its initial undisturbed state.

The same discovered interaction between neighboring pores could be expected in real porous media, buttransmitting the information of turbulent patches will be damped by going far from transitional pores.

ACKNOWLEDGMENTS

The work was partly sponsored by the Swedish Research Council. The authors acknowledge the input and discussions with Professor Håkan Gustavsson.

REFERENCES

Çengel, Y. A., & Cimbala, J. M. (2006). Fluid mechanics : Fundamentals and applications. New York: McGraw-Hill.

Chauveteau, G., &Thirriot, C. (1967). Régimes d'écoulement en milieu poreuxetlimite de la loi de darcy. La Houille Blanche, (2), 141-148.

Comiti, J., Sabiri, N. E., &Montillet, A. (2000). Experimental characterization of flow regimes in various porous media — III: Limit of darcy's or creeping flow regime for newtonian and purely viscous non-newtonian fluids. Chemical Engineering Science, 55(15), 3057-3061.

Darcy, H. (1856). Les fontain espubliques de la ville de dijon. Paris: Dalmont.

Dou, H., &Khoo, B. C. (2005). Investigation of turbulent transition in plane couetteflows using energy gradient method. ArXiv Preprint nlin/0501048,

Dupuit, J. (1863). Étudesthéoriquesetpratiquessur le mouvement des eaux. Paris: Dunod.

Dybbs, A., & Edwards, R. (1984). A new look at porous media fluid mechanics-darcy to turbulent. Fundamentals of Transport Phenomena in Porous Media, 82, 201-258.

Forchheimer, P. (1901). Wasserbewegungdurchboden. Z. Ver. Deutsch. Ing, 45(1782), 1788.

Fourar, M., Radilla, G., Lenormand, R., & Moyne, C. (2004).On the non-linear behavior of a laminar single-phase flow through two and three-dimensional porous media. Advances in Water Resources, 27(6), 669-677.

Gustavsson, L. H. (1991). Energy growth of three-dimensional disturbances in plane poiseuille flow. Journal of Fluid Mechanics, 224, 241-260.

Hassanizadeh, S. M., & Gray, W. G. (1987).High velocity flow in porous media. Transport in Porous Media, 2(6), 521-531.

Hayes, R., Afacan, A., Boulanger, B., &Shenoy, A. (1996).Modelling the flow of power law fluids in a packed bed using a volume-averaged equation of motion. Transport in Porous Media, 23(2), 175-196.

Hellstrom, J. G. I., Jonsson, P. J. P., & Lundstrom, T. S. (2010). Laminar and turbulent flowthrough an array of cylinders. Journal of Porous Media, 13(12)

Hlushkou, D., &Tallarek, U. (2006).Transition from creeping via viscous-inertial to turbulent flow in fixed beds. Journal of Chromatography A, 1126(1), 70-85.

Hubbert, M. K. (1957). Darcy's law and the field equations of the flow of underground fluids. Hydrological Sciences Journal, 2(1), 23-59.

Joseph, D. D., & Yang, B. H. (2010). Friction factor correlations for laminar, transition and turbulent flow in smooth pipes.Physica D: Nonlinear Phenomena, 239(14), 1318-1328.

Khayamyan, S., Lundström, T. S., & Gustavsson, L. H. (2014). Experimental Investigation of Transitional Flow in Porous Media with Usage of a Pore Doublet Model. Transport in Porous Media, 101(2), 333-348.

Lindquist, E. (1933). On the flow of water through porous soil. Proc., 1er Congres Des Grands Barrages, pp. 81-101.

Lundström, T. S., Gustavsson, L. H., Jēkabsons, N., & Jakovics, A. (2008). Wetting dynamics in multiscale porous media.porous pore‐doublet model, experiment and theory. AIChE Journal, 54(2), 372-380.

Ma, H., & Ruth, D. (1993). The microscopic analysis of high forchheimer number flow in porous media. Transport in Porous Media, 13(2), 139-160.

McClure, J., Gray, W., & Miller, C. (2010). Beyond anisotropy: Examining non-darcy flow in asymmetric porous media. Transport in Porous Media, 84(2), 535-548.

Muskat, M., & Wyckoff, R. D. (1946). The flow of homogeneous fluids through porous media JW Edwards Ann Arbor, Mich.

Nemec, D., &Levec, J. (2005). Flow through packed bed reactors: 1. single-phase flow. Chemical Engineering Science, 60(24), 6947-6957.

Nordlund, M., & Lundström, T. S. (2009). An investigation of particle deposition mechanisms during impregnation of dual‐scale fabrics with micro particle image velocimetry. Polymer Composites, 31(7), 1232-1240.

Panfilov, M., &Fourar, M. (2006).Physical splitting of nonlinear effects in high-velocity stable flow through porous media.Advances in Water Resources, 29(1), 30-41.

Panfilov, M., Oltean, C., Panfilova, I., &Buès, M. (2003).Singular nature of nonlinear macroscale effects in high-rate flow through porous media. ComptesRendusMecanique, 331(1), 41-48.

Papathanasiou, T., Markicevic, B., &Dendy, E. (2001).A computational evaluation of the ergun and forchheimer equations for fibrous porous media.Physics of Fluids, 13, 2795.

Reynolds, O. (1883). An experimental investigation of the circumstances which determine whether the motion of water shall be direct or sinuous, and of the law of resistance in parallel channels. Proceedings of the Royal Society of London, 35(224-226), 84-99.

Rose, W., & Witherspoon, P. A. (1956). Trapping oil in a pore doublet

Sanchez-Palencia, E. (1980). Non-homogeneous media and vibration theory.Berlin ; New York: Springer.

Scheidegger, A. E. (1958). The physics of flow through porous media. Soil Science, 86(6), 355.

Schlichting, H. (1968). Boundary-layer theory (6 ed. [3 English ed.] ed.). New York: McGraw-Hill.

Schneebeli, G. (1955). Expériences sur la limite de validité de la loi de darcy et l'apparition de la turbulence dans un écoulement de filtration. La Houille Blanche, (2), 141-149.

Seguin, D., Montillet, A., Comiti, J., &Huet, F. (1998). Experimental characterization of flow regimes in various porous media—II: Transition to turbulent regime. Chemical Engineering Science, 53(22), 3897-3909.

Skjetne, E., Hansen, A., & Gudmundsson, J. (1999). High-velocity flow in a rough fracture. Journal of Fluid Mechanics, 383, 1-28.

Skjetne, E., &Auriault, J. (1999).High-velocity laminar and turbulent flow in porous media. Transport in Porous Media, 36(2), 131-147.

Sorbie, K., Wu, Y., & McDougall, S. (1995). The extended washburn equation and its application to the oil/water pore doublet problem. Journal of Colloid and Interface Science, 174(2), 289-301.

Wan, J., Tokunaga, T. K., Tsang, C., & Bodvarsson, G. S. (1996). Improved glass micromodel methods for studies of flow and transport in fractured porous media. Water Resources Research, 32(7), 1955-1964.

Whitaker, S. (1986). Flow in porous media I: A theoretical derivation of darcy's law. Transport in Porous Media, 1(1), 3-25.

Whitaker, S. (1996). The forchheimer equation: A theoretical development. Transport in Porous Media, 25(1), 27-61.

White, F. M. (1979). Fluid mechanics (International student 3rd. ed.). Tokyo: McGraw-Hill.

Wygnanski, I., & Champagne, F. (1973).On transition in a pipe.part 1. the origin of puffs and slugs and the flow in a turbulent slug. Journal of Fluid Mechanics, 59(02), 281-335.